

# Impact of Cell Loading of Recombinant Spider Silk Based Bioinks on Gelation and Printability

Annika Lechner, Vanessa T. Trossmann, and Thomas Scheibel\*

Printability of bioinks encompasses considerations concerning rheology and extrudability, characterization of filament formation, shape fidelity, cell viability, and post-printing cellular development. Recombinant spider silk based hydrogels might be a suitable material to be used in bioinks, that is, a formulation of cells and materials to be used for bioprinting. Here, the high shape fidelity of spider silk ink is shown by bioprinting the shape and size of a human aortic valve. Further the influence of the encapsulation of cells has been evaluated on spider silk hydrogel formation, hydrogel mechanics, and shape fidelity upon extrusion based bioprinting. It is shown that the presence of cells impacts the gelation of spider silk proteins differently, depending on the used silk variant. RGD-modified spider silk hydrogels are physically crosslinked by the cells, while there is no active interaction between cells and un-tagged spider silk proteins. Strikingly, even at cell densities up to ten million cells per milliliter, cell viability is high after extrusion-based printing, which is a significant prerequisite for future applications. Shape fidelity of the printed constructs is demonstrated using a filament collapse test in the absence and presence of human cells.

## 1. Introduction

Extrusion based bioprinting is one of several advanced bottom-up tissue engineering techniques in the evolving field of biofabrication.<sup>[1]</sup> Typically, continuous strands of a hydrogel (acellular biomaterial ink) or bioink are dispensed through a nozzle in a layer-by-layer fashion.<sup>[2]</sup> Bioinks contain one or more material components functioning as mimetic scaffolds as well as cells as the living element.<sup>[3]</sup> Biofabrication enables the simultaneous deposition of cells, materials, and factors into hierarchically structured and personalized constructs.<sup>[4]</sup> Each application and processing technique requires individually optimized bioinks. On the one hand, the chosen material has to provide appropriate rheological properties, including viscosity, viscoelastic shear moduli, shear stress, and elastic recovery, suitable for the desired processing technique.<sup>[5]</sup> On the other hand, it

has to support cellular survival, proliferation, and maturation before, during, and after the printing process.<sup>[6]</sup> For bioink formulations, natural polymers are often favored over synthetic materials, as the latter can cause limitations due to toxicity, low biocompatibility and/or the lack of biological binding sites.<sup>[7]</sup> The choice of cell type dictates maturation from printed constructs to functional tissues or tissue models. However, given the nature of living cells, the interplay with the surrounding material based on, for example, porosity and stiffness or presented biological cues, significantly influences cellular development.<sup>[8]</sup> Further, mechanics and printability of the bioink are affected by interactions between the materials and the cells and potential structural disruption based thereon.<sup>[9]</sup> Evaluation of the performance of a bioink includes consideration of rheological parameters, extrudability, and filament characterization including shape fidelity during and after printing.<sup>[5]</sup> For successful bioprinting, bioinks have to display shear-thinning behavior, with the viscosity decreasing with increasing shear stress during extrusion and rising with the drop of shear stress after printing, and viscoelasticity, which can be described by the storage ( $G'$ ) and loss ( $G''$ ) modulus during oscillatory measurements. Ideally, bioinks should show a reversible, fast gel-solid transition, meaning easy flow through the nozzle during extrusion followed by rapid elastic shape retention after dispensation.<sup>[5,10]</sup> Studies looking at the effect of cells on different aspects of bioink printability elucidate the complexity of the underlying factors. For example, collagen based bioinks showed increased storage moduli and viscosities before


A. Lechner, V. T. Trossmann, T. Scheibel  
Lehrstuhl Biomaterialien, Universität Bayreuth  
Prof.-Rüdiger-Bormann Straße 1, 95447 Bayreuth, Germany  
E-mail: thomas.scheibel@bm.uni-bayreuth.de

T. Scheibel  
Bayreuther Zentrum für Kolloide und Grenzflächen (BZKG)  
Universität Bayreuth  
Universitätsstraße 30, 95440 Bayreuth, Germany

T. Scheibel  
Bayerisches Polymerinstitut (BPI)  
Universität Bayreuth  
Universitätsstraße 30, 95440 Bayreuth, Germany

T. Scheibel  
Bayreuther Zentrum für Molekulare Biowissenschaften (BZMB)  
Universität Bayreuth  
Universitätsstraße 30, 95440 Bayreuth, Germany

T. Scheibel  
Bayreuther Materialzentrum (BayMAT)  
Universität Bayreuth  
Universitätsstraße 30, 95440 Bayreuth, Germany

 The ORCID identification number(s) for the author(s) of this article can be found under <https://doi.org/10.1002/mabi.202100390>

© 2021 The Authors. Macromolecular Bioscience published by Wiley-VCH GmbH. This is an open access article under the terms of the Creative Commons Attribution-NonCommercial License, which permits use, distribution and reproduction in any medium, provided the original work is properly cited and is not used for commercial purposes.

DOI: 10.1002/mabi.202100390

gelation and decreased storage moduli after gelation with increasing chondrocyte densities. Notably, the printing resolution was increased at higher cell densities.<sup>[11]</sup> Another study looked into bioinks based on gelatin methacrylate, gelatin gum, and human endothelial cells. While higher cell densities led to increased storage and loss moduli as well as decreased flow points (stress at the  $G' = G''$  crossover point), they had no influence on the reported outcome of the printing.<sup>[12]</sup>

Amongst other natural polymers, silk based materials are employed as matrix and bioink components within biofabrication applications. They offer non-toxicity, biocompatibility, and biodegradability and can be processed into various morphologies.<sup>[7]</sup> For example, a silk fibroin solution, prepared after extraction from *Bombyx mori* cocoons, was successfully 3D printed using extrusion bioprinters and by including sacrificial particles and several post-treatment steps, hierarchical structures with tunable pore sizes were generated.<sup>[13]</sup> A cell-friendly gelation process could be achieved through the addition of the synthetic polymer polyethylene glycol (PEG) which induced  $\beta$ -sheet formation, leading to physical cross-linking without the need for post-treatment.<sup>[14]</sup> In other studies, gelatin was added to ink formulations, to enhance the rather poor mechanical properties and to tune the degradation profile of silk fibroin hydrogels.<sup>[15,16]</sup>

Hydrogels made of recombinantly produced spider silk proteins have recently been shown to be suitable as the material component of printable bioinks without the need of additives. Based on the repetitive core sequence of the European garden spider *Araneus diadematus* dragline silk fibroin 4, the protein eADF4(C16) and its integrin-binding-motif-containing variant eADF4(C16)-RGD form physically cross-linked hydrogel networks at aqueous conditions without the need for additional crosslinking.<sup>[17–19]</sup> Recombinant eADF4(C16)-based spider silk proteins self-assemble from an intrinsically disordered monomeric protein in solution into tightly packed cross- $\beta$  nanofibrils with a high  $\beta$ -sheet content via intra- and intermolecular physical interactions.<sup>[18,20,21]</sup> During fibril self-assembly, the poly-alanine stretches (Ala)<sub>8</sub> of each C-module form strong, crystalline, antiparallel  $\beta$ -sheets via hydrogen bonding, while the glycine/proline rich sequence repeats (e.g. GPGXY) remain unstructured or fold into helices or turns forming an amorphous, flexible part embedding the  $\beta$ -sheet crystallites.<sup>[18,21–23]</sup> At higher protein concentrations (above 2% (w/v)) eADF4(C16)-based spider silk proteins self-assemble into stable  $\beta$ -sheet rich hydrogels with a nanofibrillar network stabilized by intra- and intermolecular physical interactions including hydrogen bonds, hydrophobic interactions, and physical entanglement.<sup>[18,24–26]</sup> Without crosslinking, hydrogels made of recombinant spider silk proteins are stable, while displaying rather soft mechanical properties. The elastic moduli of 3% (w/v) eADF4(C16) hydrogels were determined to be in the lower kilopascal range ( $\leq 1$  kPa). This means, that hydrogels made of recombinant spider silk proteins, without additional modifications, are well suited for but also limited to the biofabrication of soft tissues. Mechanical properties can, however, be increased to reach the range of muscle, skin, and cartilage tissue,<sup>[27]</sup> using chemical cross-linking and increasing the protein concentration, which is feasible up to 7% (w/v) in aqueous solution, to strengthen the hydrogel to elastic moduli up to 110 kPa.<sup>[18]</sup> The presence of salts, by adding cell culture media to the protein solutions, resulted

in faster gelation and stiffer hydrogels.<sup>[25]</sup> Studies on different variants of the recombinant spider silk protein showed a clear influence of the RGD-tag, which has been genetically engineered into the protein, on the stiffness of hydrogels. Measured at the same protein concentration, eADF4(C16)-RGD hydrogels displayed elastic moduli of  $\approx 0.2$  kPa, compared to  $\approx 0.02$  kPa for hydrogels made eADF4(C16).<sup>[28]</sup> Consequently, the elastic moduli could be adjusted to be similar by applying different protein concentrations.<sup>[26]</sup>

The gentle gelation process allows us to simultaneously encapsulate cells within the shear-thinning, viscoelastic hydrogels for 3D bioprinting. The suitability of spider silk based bioinks to print straight-forward and cell-friendly grid structures using micro-valve printing has been previously shown.<sup>[24,26]</sup> In this study, we further assessed and improved the printability of recombinant spider silk based bioinks. To obtain optimal printing conditions, the influence of temperature on the rheological properties of eADF4(C16) hydrogels was evaluated. It was demonstrated that these hydrogels can be successfully extrusion-printed with high shape-fidelity into the shape of a human aortic heart valve without the need of any additives or chemical crosslinkers. Successful fabrication of biologically active constructs strongly relies on the ability of an ink to encapsulate high amounts of cells, while facilitating printability, cellular survival, and proliferation. Building on previous studies dealing with recombinant spider silk based bioinks, here, cell densities were increased from one million up to ten million cells per milliliter. For the first time, characterization of gelation kinetics as well as rheological evaluation was performed on cell-containing bioinks based on recombinant spider silk proteins. This study shows the ability of recombinant spider silk protein based materials to be used as high cell-content containing bioinks that are printable to yield advanced structures.

## 2. Results and Discussion

### 2.1. Printability of Recombinant Spider Silk Inks

To evaluate the previously shown potential of extrusion printing using recombinant spider silk inks<sup>[24,26,29]</sup> in terms of geometry as well as durability of the gained structures in detail, the shape of a human aortic valve (model source: Cellink) was printed (**Figure 1A**), as well as the filament collapse test was performed (**Figure 1B–D**)<sup>[30]</sup> using acellular 3% (w/v) eADF4(C16) hydrogels. Tapered needles, instead of cylindrical ones, improved the printing results for both set-ups. This might be due to reduced pressure and shear stress applied to the material in the tapered geometry,<sup>[31]</sup> preventing phase separation, which was seen during printing with cylindrical steel needles. Interestingly, the shape-fidelity of the printed human aortic valve could be confirmed using two different extrusion bioprinters, RegenHU's 3D Discovery and Cellink's BioX (**Figure 1A**). The size and shape of both constructs, as well as the amount of material needed for both prints (3 mL) were almost identical. Most apparent difference were the closed layers on the 3D Discovery's printed structure versus the open pores on the BioX's print. These varieties occurred even though all consumables, like cartridge and nozzle and basic setting, including layer height and infill pattern and density, were identical. This result demonstrated in principle the good

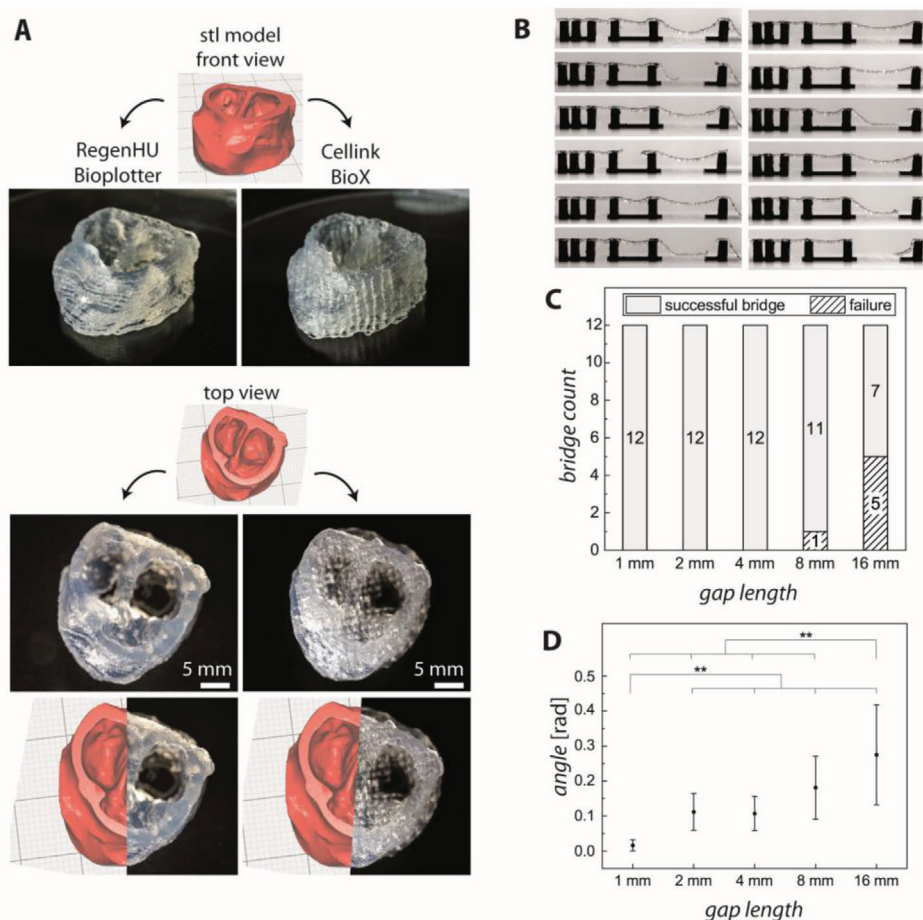


**Figure 1.** Shape fidelity of extrusion-printed spider silk hydrogels. A) As an example of printed complex scaffold structures, the shape of a human aortic valve (stl-file source: Cellink) was printed with 3% eADF4(C16) hydrogels on two different bioplotters, namely RegenHU's 3D Discovery and Cellink's BioX. B) Using a 22G tapered tip, one strand of hydrogel filament was printed over a pillar structure, and this process was repeated twelve times. Pictures were taken immediately after printing. C) The failure of the hydrogel to bridge each gap increased with increasing distance. D) Angle of deflection determined graphically from images of filament strands successfully extruded over increasingly spaced pillars (\*\* $p \leq 0.05$ ).

reproducibility when printing distinct shapes on different printers, but also showed the variation of separately acquired gcodes, meaning the printer's exact instructions, regarding details within the printed shape. Advanced features in these printed structures included overhanging walls and cavities on the inside bridged by upper layers. To quantify the durability of the printed spider silk strands, a filament collapse test was performed. One strand of hydrogel was placed over several pillars with increasing gaps in between (Figure 1B). For a realistic representation, 12 tests, including failed bridges (Figure 1C) are displayed.

The results showed that bridging with the spider silk hydrogels is reliable up to 8 mm without failing. Further, the largest gap with a length of 16 mm was bridged successfully seven out of twelve times. Strand collapses possibly occurred due to small inhomogeneities within the physically cross-linked hydrogel. The angle of deflection was determined as a measure of shape fidelity and the strands ability to hold its own weight against gravity (Figure 1D). With increasing gap size, the angle, and its deviation increased. There was no significant difference between the angles determined for 2, 4, and 8 mm gap lengths. The smallest (1 mm) and largest (16 mm) distance however, resulted in signif-

icant smaller or larger angles of deflection compared to all other distances.

eADF4(C16) hydrogels show shear thinning and viscoelastic behavior required for extrusion bioprinting independent of the used silk concentration.<sup>[18,24–26]</sup> However, during printing of the heart valve and during the filament collapse test, it became apparent that temperature has a severe impact on printability. Therefore, rheology was measured at 25 °C as previously published, but additionally at 4 and at 37 °C. With increasing temperature, higher shear-rate-dependent viscosities (Figure 2A), flow points at higher stresses (Figure 2B) and longer linear viscoelastic regions (Figure 2C) were identified. Normally, the viscosity of a sample decreases with increasing temperature. However, if a sample shows temperature dependent hardening, like the recombinant spider silk hydrogels, this effect can be reversed.<sup>[10]</sup> Generally, higher viscosities and higher yield stresses are linked to better printability, especially regarding filament formation and stiffness after printing, but are also accompanied by an increased pressure and shear stress during printing.<sup>[5]</sup> This consequence resulting from the rheological changes explained the observation made with recombinant spider silk inks. As already men-

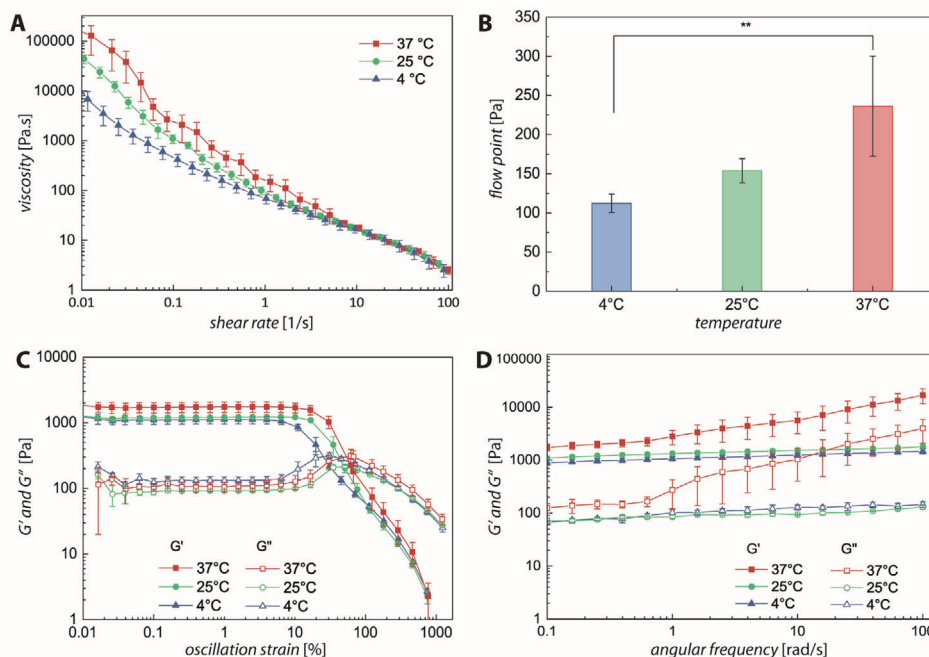


**Figure 2.** Temperature-dependent rheology of 3% eADF4(C16) hydrogels. Rheological measurements of the spider silk hydrogels were performed at 4, 25, and 37 °C. A) Viscosity was measured while increasing rotational shear rates from 0.01 to 100 s<sup>-1</sup>. B) Flow points were determined as the crossover of G' (storage modulus) and G'' (loss modulus) at constant angular frequency (10.0 rad s<sup>-1</sup>) over increase in strain from 0.01% to 1000.0% using TRIOS software (\*\**p* ≤ 0.05). C) G' and G'' at constant angular frequency (10.0 rad s<sup>-1</sup>) over an increase in strain from 0.01% to 1000.0% and D) at constant strain (1.0%) over an increase in oscillatory frequencies from 0.1 to 100 rad s<sup>-1</sup>.

tioned above, higher printing pressure led to decreased material homogeneity, occasionally causing inconstant filament extrusion. It turned out that the printing should be done, if compatible with the encapsulated cells, at room temperature. Oscillatory frequency-dependent measurements confirmed that finding (Figure 2D). While at 4 °C and at 25 °C the samples showed stability over the entire range of frequencies applied, at 37 °C a clear instability of storage and loss modulus could be detected over varying angular frequencies.

## 2.2. Gelation of Spider Silk Based Bioinks

The spider silk hydrogel variants eADF4(C16) and eADF4(C16)-RGD were compared to hydrogels made of eADF4(C16)-RGE in terms of usability in bioinks. eADF4(C16)-RGD and eADF4(C16)-RGE are identical in most physico-chemical properties and differ only in one amino acid: in eADF4(C16)-RGE, the glutamic acid (E) replaces the aspartic acid (D) of the eADF4(C16)-RGD variant. This change has a severe impact on cell binding, since the RGE peptide does not properly fit into the binding pocket of integrins yielding significantly lower binding affinities.<sup>[32]</sup> However, the total net charge as well as charge distribution remain the same. Not surprisingly, eADF4(C16)-RGE 2D films showed a similar low adhesion and proliferation of Balb 3T3 fibroblasts as eADF4(C16).<sup>[19]</sup>

In previous studies, we have already shown that eADF4(C16) and eADF4(C16)-RGD hydrogels are suitable matrix materials for cell encapsulation. Further, it has been shown that chang-

ing the protein concentration upon gelation allowed us to adjust the mechanical properties of the hydrogels.<sup>[18,24,26]</sup> Here, gelation of all three spider silk variants was investigated in the presence of RPMI media as well as, for the first time, in presence of the mammalian cell line BxPC-3 (pancreatic adenocarcinoma cell line) to analyze the respective influence on nano-fibril formation and gelation kinetics. Since gelation strongly depends on the silk variant itself, but also on the protein concentration used, it was decided to leave the protein concentrations the same (3%(w/v)) in order to focus on the influence of the silk variant on kinetics in the absence and presence of cells. To reveal the cellular impact on hydrogel formation, cells were added either directly at the beginning of the gelation process or at the end of the lag phase (i.e., nucleus formation for fibril growth followed by hydrogel formation) of spider silk assembly.<sup>[33]</sup>

Both, eADF4(C16)-RGD and eADF4(C16)-RGE displayed an accelerated fibril formation and gelation in comparison to eADF4(C16) in presence of RPMI media (Figure 3A, red curves). Interestingly, eADF4(C16)-RGE showed an increase in turbidity shortly after adding the media with a short lag-phase (≈40 min), while eADF4(C16)-RGD displayed a lag-phase of ≈100 min before exponential fibrillization started. In contrast, eADF4(C16) had the longest lag-phase of 500 min. During the lag-phase (nucleation phase) soluble, intrinsically disordered, mostly unstructured spider silk proteins (monomers) transformed into thermodynamically meta-stable β-sheet rich assemblies (oligomers) by physical interactions. These oligomers acted as nuclei for exponential fibril growth by interaction with further soluble silk monomers (fibril elongation phase) resulting in tightly packed

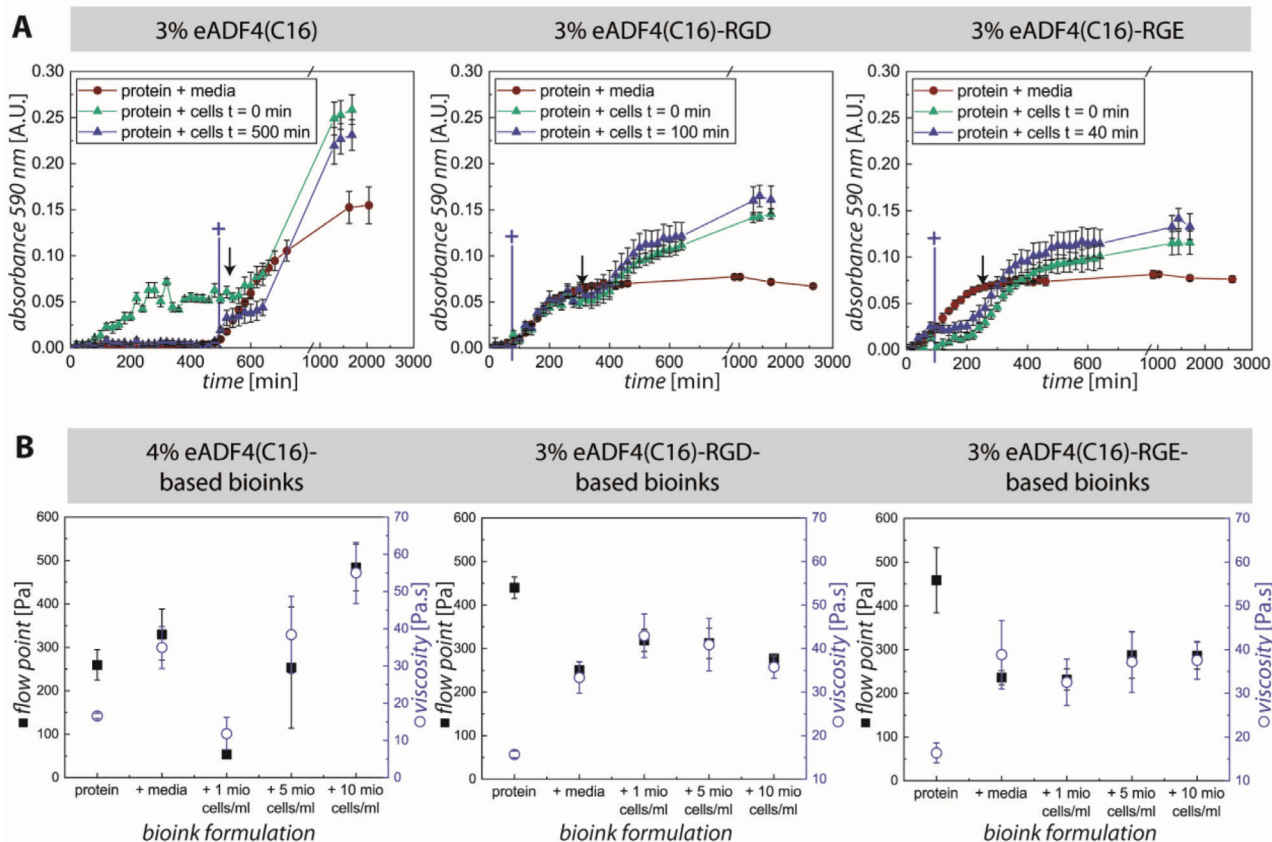


**Figure 3.** Spider silk gelation in the presence of mammalian cells. A) Protein solutions were mixed with either only media or media plus BxPC-3 cells at finally 1 million cells per milliliter. For each spider silk variant, cells were added either at the beginning of the incubation ( $t = 0$  min) or at the end of the lag phase (nucleation)/beginning of the exponential growth phase of nanofibrils ( $t = 500$  min in case of eADF4(C16),  $t = 100$  min in case of eADF4(C16)-RGD, or  $t = 40$  min in case of eADF4(C16)-RGE; marked with blue crosses). Fibrillization/gelation was quantified measuring the change in turbidity at 570 nm and 37 °C. Appropriate blank values were subtracted and first data points were normalized to zero for better comparability of the curves. Black arrows indicate the intermediate plateau of samples with cells. B) Rheological properties of 4% eADF4(C16)-based bioinks, 3% eADF4(C16)-RGD-based bioinks, and 3% eADF4(C16)-RGE-based bioinks were analyzed in the absence or presence of BxPC-3 cells (only silk protein, silk protein + 15% (v/v) media, silk protein + 1 mio cells per milliliter, 5 mio cells per milliliter or 10 mio cells per milliliter in 15% (v/v) media). Flow points were determined as crossover of storage ( $G'$ ) and loss modulus ( $G''$ ) measured at constant angular frequency ( $10.0 \text{ rad s}^{-1}$ ) over increase in strain from 0.01% to 1000.0%. Viscosity was determined at a shear rate of  $10 \text{ s}^{-1}$ .

thermodynamically stable cross- $\beta$  nanofibrils with a high  $\beta$ -sheet content.<sup>[21]</sup> The stationary phase upon completion of fibril formation and gelation was seen after 300 min for both modified variants and after 1500 min for eADF4(C16). These results indicated that both peptide tags accelerated nucleation, fibril formation, and gelation. The acceleration of gelation of eADF4(C16)-RGD and eADF4(C16)-RGE could be resulting from the additional charged amino acid residues ensuring for example ionic bonding with ions from cell culture media.<sup>[25]</sup>

The addition of BxPC-3 cells before fibrillization (Figure 3A, green curves) affected the nucleation-dependent gelation in different ways: while the initial nucleation of eADF4(C16) was apparently accelerated (shorter lag-phase), in the case of eADF4(C16)-RGE a deceleration was seen (longer lag-phase). Thus, the formation of thermodynamically meta-stable oligomers by intra- and maybe also intermolecular protein interactions was faster in the case of soluble eADF4(C16), but slower in case of eADF4(C16)-RGE. In contrast, initial fibril formation of eADF4(C16)-RGD was not influenced in the presence of cells

(identical lag-phase) indicating a similar formation of nuclei independent of cells. Interestingly, for all spider silk variants a similar course of the following exponential fibril growth phase could be detected: after a first increase in turbidity yielding an intermediate plateau (Figure 3A, black arrows), a second turbidity increase was seen until finally the stationary phase was reached. These curves indicated that soluble silk proteins docked on the pre-formed silk nuclei leading to fibril growth (first increase in turbidity). During the intermediate plateau interval, no notable fibrillization took place, and a first hydrogel network was already formed at this intermediate plateau. The second increase in turbidity could be a rearrangement of silk fibrils caused by the present cells leading to the formation of a denser packed, twisted, cell-interconnected network of silk fibrils compared to pure hydrogels without cells. This fibril-cell network would also explain the higher turbidity values of the stationary phase at the end, where gelation was completed. Looking at the single proteins, it could be seen that the exponential fibril growth of eADF4(C16)-RGD was apparently not influenced by present cells, as both

curves (with and without cells), overlapped until the intermediate plateau was reached. For eADF4(C16) and eADF4(C16)-RGE the cells caused an acceleration of fibrillization. One reason could be that the present cells minimize the free space in the solution (i.e., a virtually higher protein concentration) forcing the soluble silk proteins to interact with the already present silk nuclei (while not showing protein–cell interactions), leading to an accelerated fibril growth. However, the cells could always interact with the cell-adhesive RGD peptide, regardless of whether the protein is soluble or assembled in nuclei or fibrils. In the case of eADF4(C16)-RGD, such a cell–protein interaction could compensate the acceleration of fibril elongation.

To further analyze the cellular impact on exponential fibril growth behavior of different spider silk variants, BxPC-3 cells were added at the end of the appropriate lag-phases, where first silk nuclei were already formed (Figure 3A, blue curves, plus-sign). In this set-up, the curves overlapped with the curves where only media was contained. Interestingly, the curves after cell addition were similar to the curves where the cells were already included from the beginning. Thus, these results supported the hypothesis of cellular impact on fibril elongation and gelation given above. Nevertheless, compared to the sample without cells, it must be mentioned that in the case of eADF4(C16) and eADF4(C16)-RGE the addition of cells initially slowed down the fibril elongation (gelation), while it remained the same for eADF4(C16)-RGD. One assumption is that the addition of cells at the beginning of the exponential fibril growth phase initially effects a destruction of the already formed network of silk nuclei and fibrils. This event in turn effects a short-term deceleration of fibril elongation due to the reduced interaction of silk nuclei and soluble protein, which could be detected for eADF4(C16) and eADF4(C16)-RGE. In the case of eADF4(C16)-RGD, one assumption is that this destructive effect could be compensated by an interaction of the cells with the RGD peptide independent of whether the protein is soluble or assembled in fibrils, as it is mainly driven by an integrin–RGD interaction.

### 2.3. Rheological Properties of Spider Silk Based Bioinks

For the following analysis of the silk bioinks regarding rheological behavior, printability, and cell viability, the focus was on the composition of the bioinks, that is, the influence of medium and different cell densities on bioink performance. Therefore, in contrast to the kinetics analysis, here the mechanical properties of the spider silk matrix should be similar. As it was known from previous studies that eADF4(C16)-RGD forms stiffer hydrogels compared to eADF4(C16) at the same protein weight to volume ratio,<sup>[24]</sup> it was decided to use a concentration of 4% (w/v) for eADF4(C16) and 3% (w/v) for eADF4(C16)-RGD and eADF4(C16)-RGE to focus on the influence of the silk variant in combination with the amounts of cells introduced. Based on these concentrations, flow points and viscosities were determined (Figure 3B). Each hydrogel was analyzed upon addition of cell culture media and further upon increasing cell density (1, 5, and 10 million cells per milliliter). All three silk variant hydrogels showed an increase in viscosity upon the addition of media. While the comparable low flow point of eADF4(C16) hydrogels increased as well, the higher flow points of eADF4(C16)-RGD

and eADF4(C16)-RGE ones dropped upon the addition of media. Both, viscosity and flow point of eADF4(C16) inks dropped significantly upon the addition of cells and increased again with increasing cell densities to values higher than initially measured for the acellular hydrogels. The effect of increasing amounts of cells was lower on the flow point and viscosity of inks made of the other two variant hydrogels. While there was an initial increase in both values for eADF4(C16)-RGD inks upon addition of the lowest cell density, the values stayed in the same regime with increasing cell densities (Figure 3B). Recovery experiments focused on stabilities of storage and loss modulus at low shear rate before and after high rotational shear stress (Appendix, Figure S1, Supporting Information). The trend to recover its properties of each ink/bioink was similar to the trend seen for the flow points (with better recovery at lower flow points). For eADF4(C16), the inks without additives, as well as the sample containing one million cells per milliliter showed good recovery. Bioinks with increasing cell densities displayed decreasing ability to recover both, storage and loss moduli. In the case of eADF4(C16)-RGD and eADF4(C16)-RGE, the recovery was significantly improved upon addition of media and cells compared to samples without additives (Appendix, Figure S1, Supporting Information). This direct correlation of higher flow points and lower recovery of inks confirmed the previous observation of unfavorable filament formation related to growing flow points, in the previous case due to temperature increase (see Figure 2B).

### 2.4. Extrusion Bioprinting of Spider Silk Based Bioinks

Printability of all bioinks was assessed using the filament collapse test (Figure 4A). In the case of all eADF4(C16) and eADF4(C16)-RGD based bioinks, rheological differences could be compensated by pressure adjustments. Each of these bioinks were able to bridge all gaps (up to 16 mm) with angles of deflection in the range of 0–0.4 rad, like that determined for 3% eADF4(C16) (Figure 1D). In contrast, for eADF4(C16)-RGE based bioinks, pressure adjustments were not sufficient, since the pressure needed for continuous filament printing resulted in faster extrusion, which could not be counteracted by the maximum speed rate (20 mm s<sup>-1</sup>) of the used printer (RegenHU's 3D Discovery). Stereo microscopy images of single bridging filament strands showed the optical differences between printed hydrogels and hydrogels containing cell culture media (Figure 4B). While clear and smooth-looking filaments were printed using the hydrogels without additives, strands containing media, especially eADF4(C16) and eADF4(C16)-RGE based ones, appeared opaque, scratchy, and larger in diameter. However, these optical changes did not affect the performance during the filament collapse test (Figure 4A). During printing, the pressure was individually adjusted for optimal outcome and noted afterwards (Figure 4C). Interestingly, the applied pressure differed a lot (400–1400 mbar), but showed the same trend for bioinks made of all three protein variants.

### 2.5. Cell Viability after Extrusion Bioprinting

For biofabrication, cell survival during encapsulation, after the 3D bioprinting process, and during subsequent cultivation and

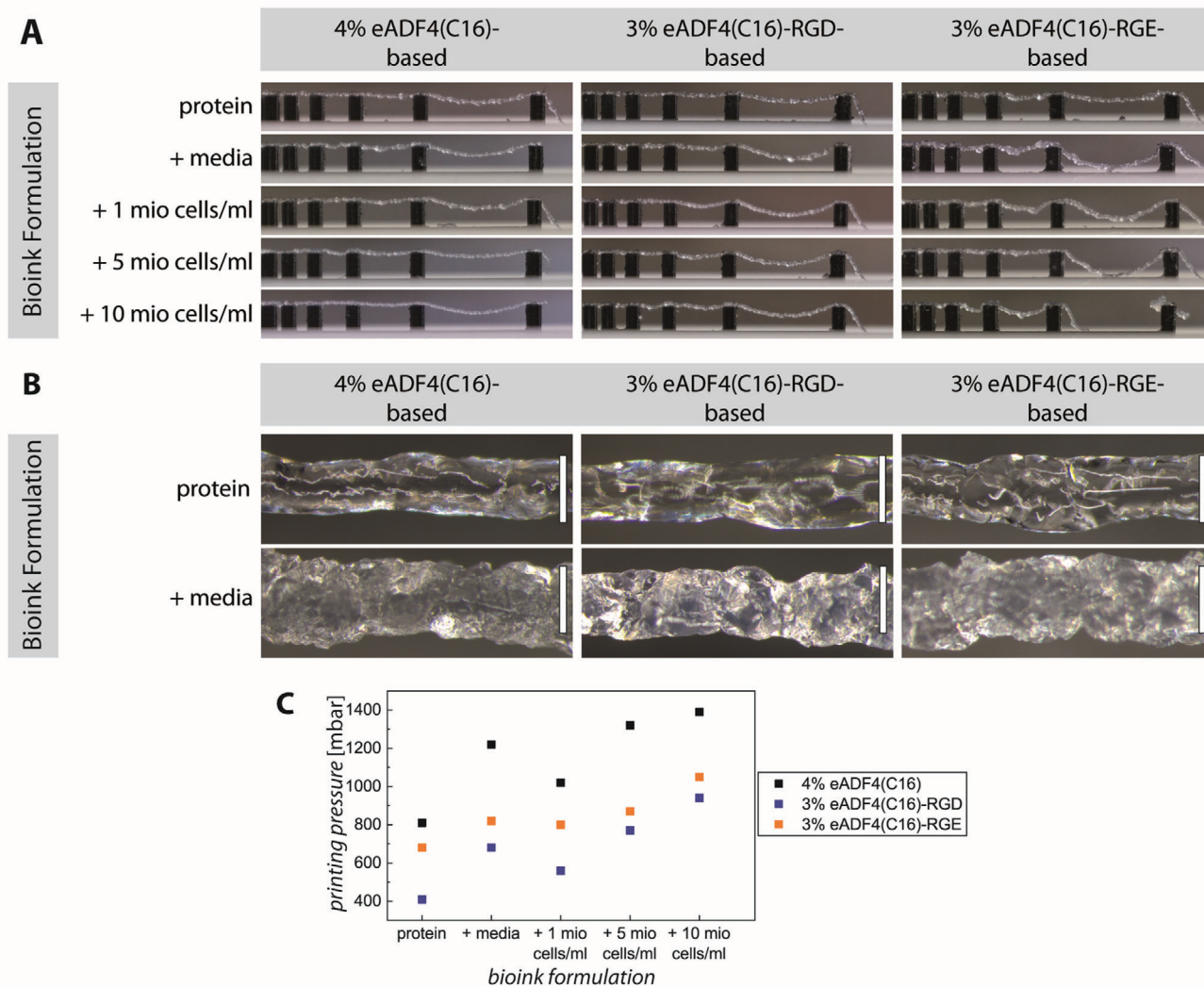


**Figure 4.** Shape fidelity of extrusion-printed spider silk bioinks. A) Using a 22G tapered tip, one strand of each bioink was printed (RegenHU's 3D Discovery) over a pillar structure; pictures were taken immediately after printing. B) Stereo microscopy images showed hanging strands between two pillars of plain spider silk hydrogels or hydrogels + media (scale bars: 200  $\mu$ m). C) The printing pressure was manually adjusted for optimal filament extrusion.

maturation is essential. Therefore, live/dead staining directly after printing and after a cultivation time of 7 and 14 days was conducted for all bioinks (Figure 5 and Figure S2, Supporting Information). Previous studies already showed that eADF4(C16) and eADF4(C16)-RGD hydrogels strongly interact with EthD-I resulting in a red-stained background signal, which is also visible in the here presented images.<sup>[24,26]</sup> The high cell survival on day 1 directly after 3D bioprinting using tapered needles (viability values for 10 mio cells per milliliter bioinks:  $85\% \pm 1\%$  for eADF4(C16),  $83\% \pm 4\%$  for eADF4(C16)-RGD, and  $75\% \pm 4\%$  for eADF4(C16)-RGE), indicated that the BxPC-3 cells survived on the one hand the encapsulation process using spider silk hydrogels and on the other hand the 3D bioprinting process. Furthermore, the cells were homogeneously distributed in all printed scaffolds without big cell clustering or aggregation. These results are highly important, as previous studies using a micro-valve printhead equipped

with a steel needle (inner diameter 0.33 mm) showed cell death rates of up to  $\approx 30\%$ , mainly during the cell encapsulation process, leading to the development of an adopted encapsulation protocol (using more media [15%]) ensuring cell survival.<sup>[24,26]</sup> Here, the combination of the adjusted and improved encapsulation protocol with cell-friendly pneumatic extrusion using tapered needles was the basis for high cell survival.

Independent of the initial encapsulated cell number, BxPC-3 cells also displayed high cell viability on day 7, however, without increase in cell number. Particularly, the smaller size of viable cells in eADF4(C16)-RGE compared to that in eADF4(C16) and eADF4(C16)-RGD scaffolds should be mentioned. Moreover, BxPC-3 cells already began to die in eADF4(C16) and especially in eADF4(C16)-RGE scaffolds after 7 days as indicated by the enhanced numbers of dead cells. This trend continued to day 14, as a higher number of viable and larger BxPC-3 cells could be

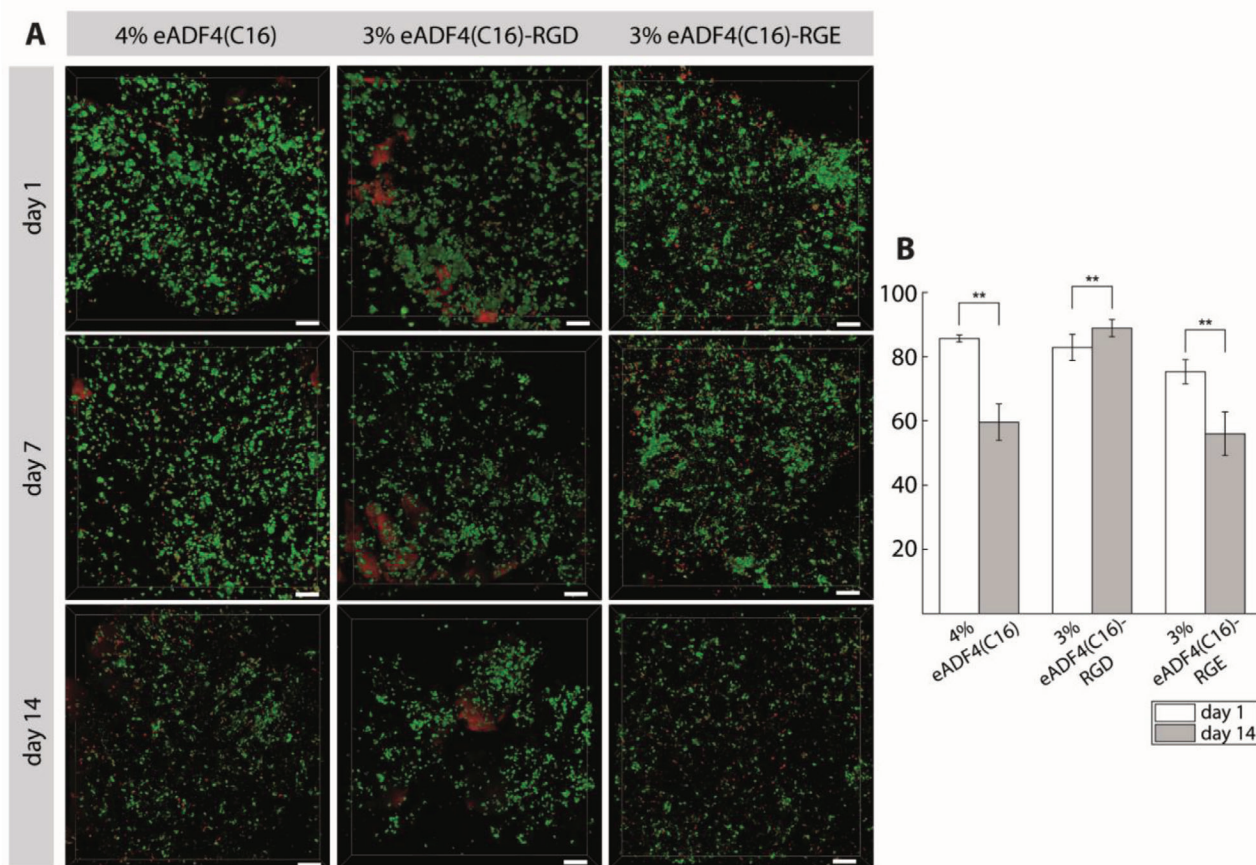


**Figure 5.** Viability of BxPC-3 cells (10 mio cells per milliliter) in printed constructs comprising 4% eADF4(C16), 3% eADF4(C16)-RGD, or 3% eADF4(C16)-RGE. Spider silk bioinks were printed using a RegenHU Bioplotter with a 22G tapered tip at room temperature and cultivated for up to 14 days at 5% CO<sub>2</sub>, 95% relative humidity, and 37 °C. A) For CLSM imaging, live cells were stained with Calcein A/M (green) and dead cells with EthD-1 (red). Background staining occurs due to interaction of hydrogels with EthD-1 (scale bars: 100 µm). B) Quantification of viable cells on day 1 and day 14 (\*\**p* ≤ 0.05).

visualized in eADF4(C16)-RGD (viability: 89% ± 3%) scaffolds compared to eADF4(C16) (viability: 60% ± 6%) and eADF4(C16)-RGE (viability: 56% ± 7%) ones, although cell proliferation could yet not be determined. The lack of cell proliferation inside 3D bioprinted spider silk scaffolds was already shown by DeSimone et al.<sup>[26]</sup> Factors could be the slow biodegradation of the recombinant spider silk matrix or changed mechanical properties after the printing process coming from structural rearrangement during shear stress.<sup>[34–38]</sup> Additionally, by using 10 million cells per milliliter, it should be analyzed whether high cell densities have a positive effect on cell survival inside the bioinks. However, the present study showed that the used silk variant had a higher impact on the cell survivability than the initial number of encapsulated cells. As the amino acid sequence of eADF4(C16) lacks any cell binding motifs,<sup>[39]</sup> the decrease in cell viability over time is not surprising. In contrast, the high cell viability of BxPC-3 cells in eADF4(C16)-RGD scaffolds could be explained by the modification with the integrin binding peptide RGD, which was recognized by cell surface receptors triggering further cellular responses. A recent *in vivo* silk vascularization study showed that surgically induced angiogenesis, indicated by the formation and sprouting of new blood vessels from an arteriovenous loop, was

clearly enhanced in implanted eADF4(C16)-RGD hydrogels compared to eADF4(C16) ones.<sup>[40]</sup> Thus, the RGD integrin binding tag is highly beneficial and necessary for successful tissue formation and growth. Nevertheless, an inadequate peptide tag, which could not interact with cell surface receptors due to steric hindrance, such as RGE, was counterproductive and led to a decreased cell interaction within the scaffold and finally cell death. It is known that RGD-resembling peptides, such as RGE, showed two to four magnitudes lower affinity to cell receptors.<sup>[32]</sup>

### 3. Conclusion

Extrusion based printing of recombinant spider silk bioinks, using tapered tips, reduces the shear stress on cells, resulting in increased cell viabilities. Our results showed that eADF4(C16) and eADF4(C16)-RGD proteins are suitable for the generation of hydrogel based bioinks with high cell densities that can be used in advanced extrusion bioprinting. Even though we saw an influence of different cell densities on rheological properties of the bioinks, we were able to adjust the procedures to accomplish reliable printing results for eADF4(C16) and eADF4(C16)-RGD based inks. For future studies, the application of different types of



cells and the examination of biological functions of printed constructs have to be studied. Even though each new bioink composition is expected to require new adjustments, valuable general insights into gelation and the interplay between cell densities, used nozzle, and applied pressure to optimize printing outcome have been gained in this study. In summary, spider silk hydrogels in bioinks show high potential for biofabrication by combining the high biocompatibility of the hydrogels with their ability for gentle cell encapsulation and reliable extrusion printing of advanced structures without the need of additives or crosslinking procedures.

## 4. Experimental Section

**Spider Silk Hydrogel Preparation:** The recombinant spider silk protein eADF4(C16) (MW: 47.7 kDa) comprises 16 repeats of a so-called C-module (sequence: GSSAAAAAAA SGPGGYGPENQGPSGPG-CYGPGGP) originating from the dragline silk of the European garden spider *A. diadematus*.<sup>[41]</sup> The modified variants eADF4(C16)-RGD (MW: 48.6 kDa) and eADF4(C16) RGE (MW: 48.6 kDa) were generated using genetic engineering.<sup>[19]</sup> While eADF4(C16)-RGD contains the integrin binding RGD sequence, the eADF4(C16)-RGE spider silk variant served as negative control. The recombinant spider silk proteins were generated as described previously.<sup>[19,41]</sup> For preparing hydrogels, the lyophilized spider silk proteins were solved in 6 M guanidinium thiocyanate (Roth, Germany) for 1 h at RT, sterile filtered (0.2  $\mu\text{m}$ , Sartorius, Germany) and dialyzed against 10 mM Tris/HCl (Roth, Germany) using dialysis membranes with a molecular weight cutoff of 6–8 kDa (Spectra/Por, Fisher Scientific GmbH, Germany) as described previously.<sup>[18,24,26]</sup> A subsequent dialysis against 25% w/v poly-ethylene glycol (MW: 20000 g mol<sup>-1</sup>, Roth, Germany) was conducted to increase protein concentrations using dialysis membranes with a molecular weight cutoff of 6–8 kDa. For subsequent experiments, protein concentrations between 30 and 50 mg mL<sup>-1</sup> were achieved. In general, hydrogels self-assembled at 37 °C overnight.<sup>[18]</sup>

**Cell Culture:** The human BxPC-3 epithelial pancreas cell line (ATCC CRL-1687), derived from an adenocarcinoma, was cultivated in RPMI-1640 medium (Sigma, Germany) supplemented with 10% v/v fetal calf serum (FCS, Biosell, Germany), 1% v/v GlutaMAX (Gibco, USA), and 0.1% v/v gentamycin sulfate (Sigma-Aldrich, Germany) at 37 °C in a humidified incubator (95% relative humidity, 5% CO<sub>2</sub>, HeraCell, Germany). BxPC-3 cells were split using 0.25% trypsin/EDTA (Gibco, USA). Cell number and viability were determined using trypan blue (Sigma-Aldrich, Germany) and an automated cell counter (BioRad, Germany).

**Preparation of Spider Silk Bioinks:** To analyze the effect of cell culture medium as well as different cell densities, acellular hydrogel samples, and bioinks were generated at 40 (4% w/v) eADF4(C16) and 30 mg mL<sup>-1</sup> (3% w/v) eADF4(C16)-RGD or eADF4(C16)-RGE. Therefore, either 47 (4.7% w/v) eADF4(C16) or 35 mg mL<sup>-1</sup> (3.5% w/v) eADF4(C16)-RGD/eADF4(C16)-RGE solutions were diluted either with 15% v/v water or RPMI medium to obtain acellular hydrogels or with 15% v/v RPMI containing BxPC-3 cells to generate respective bioinks. The solutions were filled in 3cc cartridges with appropriate pistons (both Drifton, Denmark) and sealed using a luer-lock syringe plug (Braun, Germany). For gel formation, the cartridges were fixed on an overhead shaker (Intelli-Mixer RM-2, Germany) and incubated at 37 °C overnight while rotating at 3 rpm to ensure homogenous cell distribution and to prevent sedimentation.

**Analysis of Gelation Kinetics:** Hydrogel gelation kinetics of the different spider silk proteins were analyzed in the absence and presence of cells upon turbidity changes during nanofibril self-assembly at 570 nm. Therefore, 35 mg mL<sup>-1</sup> (3.5% w/v) eADF4(C16), eADF4(C16)-RGD, and eADF4(C16)-RGE spider silk solutions were prepared using PEG dialysis as described above. For samples without cells, 15% v/v RPMI medium were added to reach a final protein concentration of 30 mg mL<sup>-1</sup> (3% w/v). 100  $\mu\text{L}$  triplicates of hydrogel solution were filled in transparent 96 well plates (Nunc, Germany) and incubated at 37 °C under a humidified atmo-

sphere in a cell culture incubator (HeraCell, Germany). The increase in turbidity indicating fibril formation was monitored at a wavelength of 570 nm using a microplate reader (Berthold, Germany) in absorbance mode. Furthermore, the impact of BxPC-3 cells, added either directly at the beginning of the gelation process or at the end of the protein-dependent lag phase, was analyzed. Therefore, BxPC-3 cells in 15% v/v RPMI were added with a concentration of one million cells per milliliter at measurement timepoint  $t = 0$  min, and  $t = 500$  min for eADF4(C16),  $t = 100$  min for eADF4(C16)-RGD, or  $t = 40$  min for eADF4(C16)-RGE.

**Rheology of Spider Silk Bioinks:** Rheological measurements were performed on a Discovery HR-2 rheometer (TA instruments, New Castle, DE, USA). Measurements were performed at 4, 25, or 37 °C as triplicates using a 25 mm plate-plate geometry with a gap of 200  $\mu\text{m}$ . Viscosity was measured either at a constant shear rate of 10 s<sup>-1</sup> or shear rate dependent from 0.01 to 100 s<sup>-1</sup>. Storage ( $G'$ ) and loss ( $G''$ ) moduli were measured at a constant strain of 1.0% at increasing oscillatory frequencies from 0.1 to 100 rad s<sup>-1</sup> or at a constant angular frequency of 10.0 rad s<sup>-1</sup>, while increasing the strain from 0.01% to 1000.0%. Flow points were determined as the crossover of  $G'$  and  $G''$  using TRIOS software. Additionally, the samples were treated twice with a constant oscillatory strain of 0.1% for 100 s each. For 400 s in between, a steady increase of rotational shear rate up to 100 s<sup>-1</sup> was applied. Recovery was recorded as stability of  $G'$  and  $G''$  at low strain before and after the higher shear rate.

**4.0.0.1. 3D Printing the Shape of Human Aortic Valves:** To demonstrate the printability of recombinant spider silk hydrogels, 3% w/v eADF4(C16) gels were printed in the size and shape of a human aortic valve (CAD-model from Cellink, Sweden). In this context, reproducibility was shown using two different models of extrusion bioprinters, BioX (Cellink, Sweden) and 3D Discovery Bioplotter (RegenHU, Villaz-Saint-Pierre, Switzerland). The stl-file was processed according to the printer's demands. For BioX, the respective G-code was generated on the device, while the 3D Discovery required an iso-file (RegenHU's G-code analogous), which was generated using the software MM Converter. For both printed constructs, the infill was set to 25% and the printing speed to 10 mm s<sup>-1</sup>. Pneumatic printheads were equipped with a 3cc cartridge, pistons (both Drifton, Denmark), and a 27G (0.2 mm inner diameter) tapered tip (Cellink, Sweden). The printing pressure was set to exactly 400 mbar on the BioX and adjusted manually for optimal printing results on the 3D Discovery (400–420 mbar). In both cases, the constructs were printed on polystyrene surfaces (Sarstaedt, Germany) and imaged using a mirrorless camera and appropriate lenses (Sony Alpha 6000, SELP1650 and SEL30M35).

**Filament Collapse Test:** The ability of a hydrogel to bridge a certain distance and its degree of collapse can be assessed using the so-called filament collapse test, where a single strand of filament was extruded over a row of pillars with defined gaps in between. The angle of deformation caused by the weight of the filament can be used for quantification.<sup>[30]</sup> The template was slightly adjusted for more convenient handling. While pillar height, size, and distance remained the same (gaps in millimeter: 1, 2, 4, 8, and 16) as published previously,<sup>[30]</sup> features were added allowing for precise positioning at the origin of the print bed, like a base plate fitting tightly on the print plate. The pillar structure was printed using an Ultimaker S5 FDM (fused-deposition-modelling) and standard PLA (poly lactic acid) filaments (Ultimaker, Netherlands). During execution of each test, one single strand of spider silk hydrogel or bioink was extruded onto individual pillar constructs (printing speed 10 mm s<sup>-1</sup>) using the 3D Discovery Bioplotter (RegenHU, Villaz-Saint-Pierre, Switzerland) equipped with a pneumatic printhead and a 22G tapered tip (Drifton, Denmark). Images of extruded strands on pillars were taken directly after printing using a mirrorless camera (Sony Alpha 6000, SELP1650) and a Leica M205C stereomicroscope, equipped with a 0.93x objective and a polarization lens in darkfield mode (Leica, Wetzlar, Germany). The angles of deflection were determined using the taken images and adobe illustrator software.

**Live/Dead Staining:** To visualize the viability of BxPC-3 cells inside the printed bioinks directly after printing (day 1) and after 7 and 14 days of cultivation, the 3D-printed spider silk scaffolds were stained using calcein acetoxymethyl ester (Calcein A/M) and ethidium homodimer I (EthD-1) (both Invitrogen, Thermo Fisher Scientific, Germany), respectively. Therefore, the printed constructs were incubated in 1x PBS containing final con-

centrations of 2  $\mu\text{M}$  Calcein A/M and 4  $\mu\text{M}$  EthD-I for 45–60 min at 37 °C in a humidified incubator containing 5% CO<sub>2</sub> (Heracell, Germany). For subsequent imaging using confocal microscopy, the staining solution was exchanged with fresh 1 $\times$  PBS. Z-stacks were recorded using a DMI 8 confocal microscope (Leica, Wetzlar, Germany) equipped with lasers using excitation wavelengths of 488 (Calcein A/M) and 552 nm (EthD-I). The viability rates of ten million cells per milliliter bioinks on day 1 and 14 were determined by quantifying live and dead cells from confocal images.

**Statistical Analysis:** To determine significance between generated data, one-way ANOVA with significance level of  $p \leq 0.05$  were performed.

## Supporting Information

Supporting Information is available from the Wiley Online Library or from the author.

## Acknowledgements

A.L. and V.T.T. contributed equally to this work. The authors acknowledge the funding from the Deutsche Forschungsgemeinschaft (DFG, German Research Foundation)-project number 326998133-TRR225 (funded sub-project: C01 TS) and SCHE603/24-1. Support from the Elite Network of Bavaria is also acknowledged.

Open access funding enabled and organized by Projekt DEAL.

## Conflict of Interest

The authors declare the following competing financial interest: T.S. is co-founder and shareholder of AMSilk GmbH.

## Data Availability Statement

The data that support the findings of this study are available from the corresponding author upon reasonable request.

## Keywords

biofabrication, bioprinting, gelation kinetics, physical crosslinking, rheology

Received: September 27, 2021

Revised: November 19, 2021

Published online: December 19, 2021

- [1] W. Sun, B. Starly, A. C. Daly, J. A. Burdick, J. Groll, G. Skeldon, W. Shu, Y. Sakai, M. Shinohara, M. Nishikawa, J. Jang, D.-W. Cho, M. Nie, S. Takeuchi, S. Ostrovidov, A. Khademhosseini, R. D. Kamm, V. Mironov, L. Moroni, I. T. Ozbolat, *Biofabrication* **2020**, 12, 022002.
- [2] L. Moroni, T. Boland, J. A. Burdick, C. De Maria, B. Derby, G. Forgacs, J. Groll, Q. Li, J. Malda, V. A. Mironov, C. Mota, M. Nakamura, W. Shu, S. Takeuchi, T. B. F. Woodfield, T. Xu, J. J. Yoo, G. Vozzi, *Trends Biotechnol.* **2018**, 36, 384.
- [3] J. Groll, T. Boland, T. Blunk, J. A. Burdick, D.-W. Cho, P. D. Dalton, B. Derby, G. Forgacs, Q. Li, V. A. Mironov, L. Moroni, M. Nakamura, W. Shu, S. Takeuchi, G. Vozzi, T. B. F. Woodfield, T. Xu, J. J. Yoo, J. Malda, *Biofabrication* **2016**, 8, 013001.
- [4] L. Moroni, J. A. Burdick, C. Highley, S. J. Lee, Y. Morimoto, S. Takeuchi, J. J. Yoo, *Nat. Rev. Mater.* **2018**, 3, 21.
- [5] A. Schwab, R. Levato, M. D'Este, S. Piluso, D. Eglin, J. Malda, *Chem. Rev.* **2020**, 120, 11028.
- [6] R. Levato, T. Jungst, R. G. Scheuring, T. Blunk, J. Groll, J. Malda, *Adv. Mater.* **2020**, 32, 1906423.
- [7] V. J. Neubauer, A. Döbl, T. Scheibel, *Materials* **2021**, 14, 674.
- [8] J. Li, C. Wu, P. K. Chu, M. Gelinsky, *Mater. Sci. Eng., R* **2020**, 140, 100543.
- [9] K. Hölzl, S. Lin, L. Tytgat, S. Van Vlierberghe, L. Gu, A. Ovsianikov, *Biofabrication* **2016**, 8, 032002.
- [10] T. G. Mezger, *The Rheology Handbook*, 4th ed., Vincentz Network, Hannover **2014**.
- [11] N. Diamantides, C. Dugopolski, E. Blahut, S. Kennedy, L. J. Bonassar, *Biofabrication* **2019**, 11, 045016.
- [12] G. J. Gillispie, A. Han, M. Uzun-Per, J. Fisher, A. G. Mikos, M. K. K. Niazi, J. J. Yoo, S. J. Lee, A. Atala, *Tissue Eng., Part A* **2020**, 26, 1349.
- [13] M. R. Sommer, M. Schaffner, D. Carnelli, A. R. Studart, *ACS Appl. Mater. Interfaces* **2016**, 8, 34677.
- [14] Z. Zheng, J. Wu, M. Liu, H. Wang, C. Li, M. J. Rodriguez, G. Li, X. Wang, D. L. Kaplan, *Adv. Healthcare Mater.* **2018**, 7, 1701026.
- [15] W. Shi, M. Sun, X. Hu, B. Ren, J. Cheng, C. Li, X. Duan, X. Fu, J. Zhang, H. Chen, Y. Ao, *Adv. Mater.* **2017**, 29, 1701089.
- [16] S. Das, F. Pati, Y.-J. Choi, G. Rijal, J.-H. Shim, S. W. Kim, A. R. Ray, D.-W. Cho, S. Ghosh, *Acta Biomater.* **2015**, 11, 233.
- [17] S. Rammensee, D. Huemmerich, K. D. Hermanson, T. Scheibel, A. R. Bausch, *Appl. Phys. A* **2006**, 82, 261.
- [18] K. Schacht, T. Scheibel, *Biomacromolecules* **2011**, 12, 2488.
- [19] S. Wohlrab, S. Müller, A. Schmidt, S. Neubauer, H. Kessler, A. Leal-Egaña, T. Scheibel, *Biomaterials* **2012**, 33, 6650.
- [20] U. Slotta, S. Hess, K. Spieß, T. Stromer, L. Serpell, T. Scheibel, *Macromol. Biosci.* **2007**, 7, 183.
- [21] M. Humenik, M. Magdeburg, T. Scheibel, *J. Struct. Biol.* **2014**, 186, 431.
- [22] K. Spieß, S. Wohlrab, T. Scheibel, *Soft Matter* **2010**, 6, 4168.
- [23] C. B. Borkner, S. Lentz, M. Müller, A. Fery, T. Scheibel, *ACS Appl. Polym. Mater.* **2019**, 1, 3366.
- [24] K. Schacht, T. Jüngst, M. Schweinlin, A. Ewald, J. Groll, T. Scheibel, *Angew. Chem., Int. Ed.* **2015**, 54, 2816.
- [25] E. DeSimone, K. Schacht, T. Scheibel, *Mater. Lett.* **2016**, 183, 101.
- [26] E. DeSimone, K. Schacht, A. Pellert, T. Scheibel, *Biofabrication* **2017**, 9, 044104.
- [27] N. R. Raia, M. McGill, T. Marcet, S. E. V. Yucha, D. L. Kaplan, 2.6.8 – *Soft Tissue Engineering in Biomaterials Science (Fourth Edition)* (Eds: W. R. Wagner, S. Sakiyama-Elbert, G. Zhang, M. Yaszemski), Academic Press, Cambridge **2020**, pp. 1399–1414.
- [28] K. Schacht, T. Jüngst, M. Schweinlin, A. Ewald, J. Groll, T. Scheibel, *Angew. Chem., Int. Ed.* **2015**, 54, 2816.
- [29] S. Kumari, H. Bargel, M. U. Anby, D. Lafargue, T. Scheibel, *ACS Biomater. Sci. Eng.* **2018**, 4, 1750.
- [30] A. Ribeiro, M. M. Blokzijl, R. Levato, C. W. Visser, M. Castilho, W. E. Hennink, T. Vermonden, J. Malda, *Biofabrication* **2017**, 10, 014102.
- [31] M. Li, X. Tian, D. J. Schreyer, X. Chen, *Biotechnol. Prog.* **2011**, 27, 1777.
- [32] U. Hersel, C. Dahmen, H. Kessler, *Biomaterials* **2003**, 24, 4385.
- [33] M. Humenik, M. Drechsler, T. Scheibel, *Nano Lett.* **2014**, 14, 3999.
- [34] S. Müller-Herrmann, T. Scheibel, *ACS Biomater. Sci. Eng.* **2015**, 1, 247.
- [35] T. B. Aigner, E. DeSimone, T. Scheibel, *Adv. Mater.* **2018**, 30, 1704636.
- [36] S. Salehi, K. Koeck, T. Scheibel, *Molecules* **2020**, 25, 737.
- [37] D. Steiner, G. Lang, L. Fischer, S. Winkler, T. Fey, P. Greil, T. Scheibel, R. E. Horsch, A. Arkudas, *Tissue Eng., Part A* **2019**, 25, 1504.
- [38] D. Pasqui, M. De Cagna, R. Barbucci, *Polymers* **2012**, 4, 1517.
- [39] A. Leal-Egaña, G. Lang, C. Mauerer, J. Wickinghoff, M. Weber, S. Geimer, T. Scheibel, *Adv. Eng. Mater.* **2012**, 14, B67.
- [40] D. Steiner, S. Winkler, S. Heltmann-Meyer, V. Trossmann, T. Fey, T. Scheibel, R. E. Horsch, A. Arkudas, *Biofabrication* **2021**, 13, 045003.
- [41] D. Huemmerich, C. W. Helsen, S. Quedzuweit, J. Oschmann, R. Rudolph, T. Scheibel, *Biochemistry* **2004**, 43, 13604.